

# PRELIMINARY LEAF AREA INDEX ESTIMATES FROM AIRBORNE SMALL FOOTPRINT FULL-WAVEFORM LIDAR DATA

Karolina D. Fieber<sup>1</sup>, Ian J. Davenport<sup>2</sup>, Mihai A. Tanase<sup>3</sup>, James M. Ferryman<sup>1</sup>, Robert J. Gurney<sup>2</sup>, Jeffrey P. Walker<sup>4</sup>, Jorg M. Hacker<sup>5</sup>

<sup>1</sup>University of Reading, School of Systems Engineering, Whiteknights, Reading, RG6 6AY, UK

<sup>2</sup>University of Reading, School of Mathematical and Physical Sciences, Harry Pitt Building, Reading, RG6 6AL, UK

<sup>3</sup>University of Melbourne, Parkville, Melbourne, 3010 VIC, Australia

<sup>4</sup>Monash University, Department of Civil Engineering, Clayton, Melbourne, VIC 3800, Australia

<sup>5</sup>Airborne Research Australia, School of the Environment, Flinders University, Adelaide, SA 5001, Australia

## ABSTRACT

This study has compared preliminary estimates of effective leaf area index (LAI) derived from fish-eye lens photographs to those estimated from airborne full-waveform small-footprint LiDAR data for a forest dataset in Australia. The full-waveform data was decomposed and optimized using a trust-region-reflective algorithm to extract denser point clouds. LAI LiDAR estimates were derived in two ways (1) from the probability of discrete pulses reaching the ground without being intercepted (point method) and (2) from raw waveform canopy height profile processing adapted to small-footprint laser altimetry (waveform method) accounting for reflectance ratio between vegetation and ground. The best results, that matched hemispherical photography estimates, were achieved for the waveform method with a study area-adjusted reflectance ratio of 0.4 (RMSE of 0.15 and 0.03 at plot and site level, respectively). The point method generally overestimated, whereas the waveform method with an arbitrary reflectance ratio of 0.5 underestimated the fish-eye lens LAI estimates.

**Index Terms**— Full-waveform, LiDAR, Leaf area index (LAI), Canopy height profile, Small-footprint

## 1. INTRODUCTION

Small footprint full-waveform LiDAR data have become increasingly available in recent years. Recording of the whole backscattered signal at regular time intervals of typically 1ns gives the possibility to adjust the off-line processing to the user's needs and provides detailed information on target distribution along the laser line-of-sight. These type of data find their major application in vegetation studies, as these are areas where the most multiple returns are triggered and where information about structure is of great value and interest for biogeoscience applications.

Several studies attempted to describe vegetation structure using full-waveform laser data. Lefsky et al. [1]

presented canopy height profile and canopy volume methods to characterize the total volume and spatial organization of foliage and gaps within the forest canopy applied to LiDAR large footprint data. Harding et al. [2] expanded and modified the canopy height profile method and applied it to the same type of data.

This study follows the assumptions and general steps presented in [2] but modifying and adapting them to small-footprint RIEGL LMS-Q560 data. Leaf area index (LAI) estimates (one sided leaf surface area per unit ground area) and canopy description accounting for occlusions and energy decrease with increasing range were derived in this way. The LAI estimates from raw waveform were then compared to LiDAR discrete points and to fish-eye lens photography LAI estimates. Since neither LiDAR nor fish-eye photography distinguishes between woody and foliar elements, the LAI estimates considered in this paper may be referred to as plant area index (PAI).

## 2. STUDY AREA AND DATA

The study area is located in New South Wales in Australia, in the Gillenbah forest, near the town of Narrandera. The most common tree species in the forest is White Cypress Pine (*Callitris glaucophylla*) with occasional Grey Box (*Eucalyptus microcarpa*) in Site 1, 10 and 17 and Monterey Pine (*Pinus radiata*) present only in Site 1.

Twelve sites were measured in the field. Each site consisted of five circular plots (12.62m radius): one in the centre (C) and one at approximately each cardinal direction (N, S, E, W). All trees with diameter at breast height (DBH) larger than 5cm within the plot limits were measured. The field measurements included tree height, crown base height, location, DBH and species. Terrestrial photographs and upward-pointing fish-eye lens photographs were also taken. Effective LAI was calculated from fish-eye lens photographs taken in the centre and in the four cardinal directions of each plot, with the final LAI value computed as the average of five photographs. The LAI for the whole site was calculated as an average of plot level LAI

measurements in each site. The fish-eye LAI estimates were obtained using HemiView software by computing the fraction of sky obscured by vegetation. In this study preliminary results for four out of twelve sites are presented. The clumping effect of canopy elements was at this stage neglected.

The LiDAR data were acquired by Airborne Research Australia on September 6<sup>th</sup> 2011 with a full-waveform RIEGL LMS-Q560 instrument as part of The Third Soil Moisture Active Passive Experiment (SMAPEX-3) [3]. The laser instrument was mounted on a light aircraft and flown at 350m above ground level (AGL) resulting in 0.175m footprint diameter and an average point spacing of 9.5 points/m<sup>2</sup>. Both transmitted and received waveforms were recorded and sampled with a frequency of 1GHz (1 nanosecond spacing). The LiDAR data corresponding to field measurements at plot and site level were extracted from the swaths of data for each of the four sites.

### 3. METHODS

#### 3.1. Gaussian decomposition

All LiDAR datasets were processed to detect peaks and optimised with the trust-region-reflective algorithm. A custom Gaussian decomposition procedure was used to detect weak returns, so as to provide more complete structure of the vegetation. The details of the procedure can be found in [4]. In order to enable further analysis and comparison to other datasets the data was calibrated and the backscattering coefficient [5] was calculated for each return. Backscattering coefficient was used to help separate ground returns from other returns in order to generate a Digital Terrain Model (DTM) for each site. Gaussian decomposition provided point clouds of XYZ coordinates with additional attributes for each plot and site. The elevations were then normalized by the DTM in order to obtain relative values.

#### 3.2. Discrete Point LAI estimation

Discrete point LAI was calculated from the points extracted from waveforms. The probability (P) of pulses reaching the ground without being intercepted was calculated as the number of single-peak waveforms returned from the ground ( $S_g$ ) to the total number of waveforms incident on the area of interest (N). The LAI was then calculated as the negative natural logarithm of this probability [6] according to:

$$PT\ LAI = -\ln(P) = -\ln\left(\frac{S_g}{N}\right) \quad (1)$$

#### 3.3. Canopy Height Profile and ‘Waveform LAI’

The received waveforms as well as the DTM and location of the peaks were used to generate a canopy height profile (CHP). The CHP generation was performed in five stages:

waveform alignment, return energy profile, canopy closure profile, cumulative leaf (plant) area profile and canopy height profile. In comparison to large footprint laser scanning data, small footprint laser waveforms do not always have a ground return. Due to that fact CHP processing cannot be applied to those waveforms and therefore they would have to be excluded from the processing, which may subsequently bias the results. To avoid that, the data were aggregated during the returned energy calculation to provide one profile for the whole dataset whether plot or site.

##### 3.2.1. Waveform-alignment

Because of slight ground level differences across the sites, the waveforms needed to be aligned according to their elevation above ground level first. In order to do so, the XYZ coordinates of the last peak in the waveform train were computed, and the DTM points within 0.5m proximity of that point used to calculate the local mean ground elevation. The optimised noise level was subtracted from the raw waveforms and the beginning and end of the waveforms found. The relative elevation of the beginning of the waveform was then calculated and matched with the elevation of the appropriate 15cm bin in the height array.

##### 3.2.2. Returned energy

The area underneath each waveform graph was calculated separately for each bin as the area of a trapezium. This area (intensity) was then output to the array of appropriate height bins. Subsequently, a mean intensity value per bin for the dataset was computed. Due to the difference in reflectance between vegetation and ground at the laser wavelength (ground is approximately twice as reflective as vegetation), the value of bins corresponding to ground return were then multiplied by 0.5 (WF0.5). The same reflectance ratio was tested in [7], who also used data acquired at 1550nm, nevertheless the authors proved that using locally-adjusted reflectance ratio delivers better results. Thus, an attempt to adjust the ratio to the specifics of the study area was undertaken. The soil in the study area region is mostly a mixture of sand, silt and clay [3]. According to [8] those soil types have the following reflectance at 1550nm: 0.52, 0.64, 0.44, respectively. Taking the average of those values and estimating the typical vegetation reflectance at 1550m from [8] the ratio between vegetation and ground was found to be 0.4 rather than 0.5. A variant of waveform method was therefore examined with 0.4 as the reflectance ratio (WF0.4). All this led to a single profile of the energy returned from a dataset for each reflectance ratio tested.

##### 3.2.3. Canopy Closure

The graph of the returned energy was processed to obtain canopy closure. First, the ground return was separated from the canopy part of the graph. Second, cumulative area underneath the energy graph from the top of the vegetation layer was calculated and normalized by the total cumulative area (including ground return).

### 3.2.4. Leaf/plant area index

To correct the effect of occlusion, the profile of canopy closure was transformed into a LAI graph by using natural logarithm and canopy closure (Eq. 2), which represents a fraction of sky obscured by the vegetation [1]. The last vegetation bin's value was treated as total LAI.

$$WF\ LAI = -\ln(1 - closure) \quad (2)$$

### 3.2.5. Canopy height profile

Canopy height profile was computed by converting normalized LAI into incremental height distribution. The CHP represents the relative vertical distribution of canopy components [2]. CHP will not be presented and discussed here further as it will be a subject of another publication.

## 4. RESULTS AND DISCUSSION

Tables 1 to 6 summarise the LAI estimates obtained by the two LiDAR methods: WF0.5/0.4 – waveform method with 0.5/0.4 reflectance ratio and PT – discrete point method, and compare them to fish-eye lens estimates (FEye). Site level LiDAR LAI values were generated in two ways: (a) as an average of plot level estimates (WFA0.5/0.4, PTA) to enable direct comparison to fish-eye site level LAI (Table 5) and (b) from processing LiDAR data over the whole site (50m radius centred at central plot) (Table 6).

In general, the WF0.5 method underestimates, whereas the PT method overestimates LAI in comparison to fish-eye lens values at the plot level (Figure 1, left). The RMSE for plots vary between 0.14-0.21 for WF0.5 and between 0.24-0.36 for PT method depending on the site. Changing the reflectance ratio to 0.4 (WF0.4) in most cases lowers the RMSE (0.05-0.21). If all 20 plots are considered together the RMSE at plot level is 0.17 for WF0.5, 0.15 for WF0.4 and 0.31 for PT. The  $R^2$  for waveform methods is 0.51, whereas for point method it drops to 0.40 (Figure 1, left). The correlation between the data is thus moderate.

At the site level the underestimation of WF0.5 method and overestimation of PT method is also evident. The RMSE at site level is much lower than that of plot level with 0.10/0.12 for WFA/WF0.5 and 0.22/0.17 for PTA/PT methods depending on the way site level LAIs are derived. Using the lower reflectance ratio (WF0.4) significantly improves estimates at the site level, which no longer exceed  $\pm 10\%$  of fish-eye LAI value. The RMSE also drops drastically to 0.03/0.05 (WFA/WF0.4). The  $R^2$  values improve as well at the site level, reaching 0.95/0.84 for WFA/WF0.4, 0.95/0.69 for WFA/WF0.5 and 0.66/0.63 for PTA/PT depending on the way site level estimates are derived (Figure 1, right). The sample is very small though so those values need to be considered with caution. As expected, averaged plot-level LAIs (a), match better fish-eye lens estimates (with the exception of PT method).

Furthermore, all LiDAR estimates for Site 1 are exceptionally close to fish-eye LAI value (within  $\pm 10\%$ ). This may be due to the fact that the fish-eye estimates for

that site were derived in a different way. Two transects of six fish-eye photos each, along North-South and East-West direction were taken and used to estimate the site level LAI value rather than using the average of plot level LAIs. The fact that they agree so closely with LiDAR estimates suggests that this method of field measurement may be more suitable for site level LAI estimates for this study area.

**Table 1. Comparison of LAI for plots in Site 1**

1	FEye	WF0.5	WF0.4	PT
C	0.84	0.46 (-46%)	0.55 (-34%)	0.44 (-48%)
E	0.64	0.62 (-3%)	0.75 (+16%)	0.72 (+11%)
N	0.54	0.61 (+14%)	0.73 (+36%)	0.83 (+54%)
S	0.31	0.50 (+63%)	0.60 (+96%)	0.51 (+65%)
W	0.61	0.47 (-23%)	0.56 (-7%)	0.58 (-5%)
RMSE		0.21	0.21	0.24

**Table 2. Comparison of LAI for plots in Site 10**

10	FEye	WF0.5	WF0.4	PT
C	0.82	0.73 (-11%)	0.87 (+5%)	1.25 (+51%)
E	0.67	0.54 (-19%)	0.65 (-3%)	0.97 (+44%)
N	0.82	0.63 (-23%)	0.75 (-8%)	1.21 (+48%)
S	0.70	0.60 (-13%)	0.72 (+3%)	1.15 (+65%)
W	0.68	0.51 (-25%)	0.62 (-10%)	0.83 (+22%)
RMSE		0.14	0.05	0.36

**Table 3. Comparison of LAI for plots in Site 17**

17	FEye	WF0.5	WF0.4	PT
C	0.72	0.72 (-0%)	0.85 (+18%)	1.06 (+47%)
E	1.00	0.60 (-40%)	0.72 (-29%)	0.77 (-23%)
N	0.76	0.57 (-25%)	0.68 (-10%)	0.84 (+11%)
S	0.64	0.69 (+8%)	0.81 (+28%)	1.01 (+59%)
W	0.58	0.57 (-1%)	0.68 (+18%)	0.81 (+41%)
RMSE		0.20	0.17	0.27

**Table 4. Comparison of LAI for plots in Site 23**

23	FEye	WF0.5	WF0.4	PT
C	0.35	0.34 (-4%)	0.41 (+18%)	0.44 (+24%)
E	0.87	0.62 (-29%)	0.74 (-15%)	0.95 (+9%)
N	0.82	0.67 (-19%)	0.79 (-3%)	1.55 (+89%)
S	0.33	0.25 (-23%)	0.33 (-1%)	0.40 (+21%)
W	0.19	0.28 (+47%)	0.35 (+81%)	0.37 (+91%)
RMSE		0.14	0.10	0.25

**Table 5. Comparison of averaged plot LAI for each site**

SITE	FEye	WFA0.5	WFA0.4	PTA
1	0.59	0.53 (-10%)	0.64 (+9%)	0.61 (+4%)
10	0.74	0.61 (-18%)	0.72 (-2%)	1.08 (+46%)
17	0.74	0.63 (-15%)	0.75 (+1%)	0.90 (+22%)
23	0.51	0.43 (-16%)	0.52 (+2%)	0.74 (+44%)
RMSE		0.10	0.03	0.22

**Table 6. Comparison of LAI at site level (whole site)**

SITE	FEye	WF0.5	WF0.4	PT
1	0.59	0.53 (-10%)	0.64 (+9%)	0.62 (+5%)
10	0.74	0.56 (-24%)	0.67 (-10%)	0.98 (+33%)
17	0.74	0.60 (-19%)	0.71 (-3%)	0.87 (+18%)
23	0.51	0.44 (-14%)	0.54 (+4%)	0.71 (+39%)
RMSE		0.12	0.05	0.17

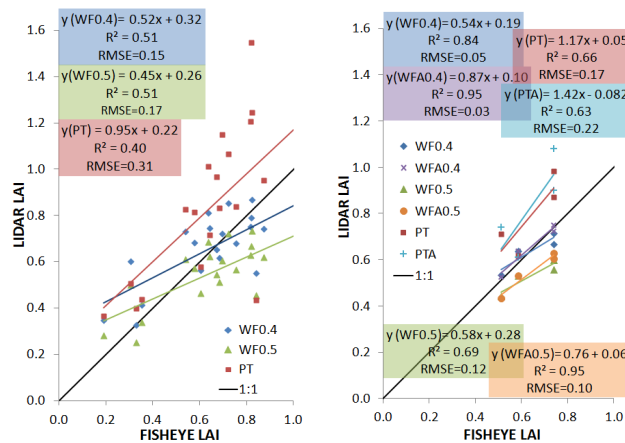


Figure 1. Comparison of LiDAR to Fish-eye LAI estimates. Left - plot level; Right - site level

The reason why the point method overestimates LAI so significantly may be because the definition of LAI depends on the point passing through the canopy to the ground to have a zero area cross-section. In reality the laser beam has a finite cross-section and is therefore, more likely to be intercepted by vegetation, causing an increase in the calculated LAI. Furthermore, the point method does not take into account the intensity of the pulses and treats all of them equally, therefore, the proportion of area of incidence is not taken into account. Another thing worth considering is that the LAI values over the site of interest are very low. Thus, even small fluctuations in LAI estimates due to errors in decomposition and changes in the number of identified single peak waveforms reaching ground will have a higher impact on the point-method derived LAI than in the case of denser forest with higher LAI values.

On the other hand, fish-eye photography is believed to underestimate LAI of coniferous canopies due to clumping effect [9]. Thus, one could conclude that point method could be closer to real LAI values. Nevertheless, neither the fish-eye nor the LiDAR are corrected for this effect therefore this should not affect the results of effective LAI. The waveform method, especially with study area-adjusted reflectance ratio, provides the results most closely matching those of fish-eye.

## 6. CONCLUSIONS

This study presents a procedure to derive effective LAI, adapted to small footprint airborne full-waveform LiDAR data. As a result waveform LiDAR LAI estimates are derived and compared to discrete point LiDAR and fish-eye lens photography LAI estimates. The discrete point method is based on points extracted from the waveform in the process of Gaussian decomposition and typically provides much higher estimates in comparison to the fish-eye method (RMSE of 0.31 and 0.22 at plot and site level, respectively). The waveform method, based on the raw light curve of waveforms, depending on the reflectance ratio between

vegetation and ground, provides similar estimates to the fish-eye photo technique with some degree of underestimation when an arbitrary reflectance ratio of 0.5 is used (RMSE of 0.17 and 0.10 at plot and site level, respectively). With the study area-adjusted ratio, the RMSE drops to 0.15 at plot and to 0.03 at site level.

In practice, LAI is still very difficult to measure and fish-eye lens estimates cannot be taken as absolute truth. They strongly depend on where the photograph is taken and should also be corrected for the clumping effect. Future work will focus on examining the remaining sites to provide larger and more reliable samples and on investigating the influence of plot-adjusted (or even smaller area) reflectance ratios between vegetation and ground on LAI estimates. Correction for the clumping effect will also be explored. Waveform LiDAR light curves representing vertical distribution of foliage should provide alternative and more representative estimates of LAI than hemispherical photography because of their continuous spatial coverage.

## 7. ACKNOWLEDGMENTS

This work was funded by EPSRC (grant number: EP/P505682/1), School of Mathematical and Physical Sciences and School of Systems Engineering of University of Reading. The authors would like to thank the National Centre for Earth Observation for funding for the waveform processing. LiDAR data collection through an Australian Research Council project FS100100040 is also acknowledged.

## 8. REFERENCES

- [1] M.A. Lefsky, et al., "Lidar Remote Sensing of the Canopy Structure and Biophysical Properties of Douglas-Fir Western Hemlock Forests". *Remote Sensing of Environment* 70 (3), pp. 339-361, 1999.
- [2] D.J. Harding, et al., "Laser altimeter canopy height profiles: methods and validation for closed-canopy, broadleaf forests". *Remote Sensing of Environment* 76 (3), pp. 283-297, 2001.
- [3] A. Monerris, et al., *The Third Soil Moisture Active Passive Experiment. Workplan.*, 2011.
- [4] K.D. Fieber, et al., "Analysis of full-waveform LiDAR data for classification of an orange orchard scene". *ISPRS Journal of Photogrammetry and Remote Sensing*, pp., (in press).
- [5] W. Wagner, "Radiometric calibration of small-footprint full-waveform airborne laser scanner measurements: Basic physical concepts". *ISPRS Journal of Photogrammetry and Remote Sensing* 65 (6), pp. 505-513, 2010.
- [6] R.H. MacArthur and J.W. MacArthur, "On Bird Species Diversity". *Ecology* 42 (3), pp. 594-598, 1961.
- [7] J. Armston, et al., "Direct retrieval of canopy gap probability using airborne waveform lidar". *Remote Sensing of Environment* 134 (0), pp. 24-38, 2013.
- [8] D. Bowker, et al., *Spectral Reflectances of Natural Targets for Use in Remote Sensing Studies*, NASA RP-1139, 1985.
- [9] F. Morsdorf, et al., "Estimation of LAI and fractional cover from small footprint airborne laser scanning data based on gap fraction". *Remote Sensing of Environment* 104 (1), pp. 50-61, 2006.